Original article

α-Glucosidase inhibitory potential of *Oroxylum indicum* using molecular docking, molecular dynamics, and *in vitro* evaluation

Check for updates

Samhita Bhaumik [a], Alekhya Sarkar [b], Sudhan Debnath [c,*], Bimal Debnath [b,*], Rajat Ghosh [d], Magdi E.A. Zaki [e], Sami A. Al-Hussain [e]

[a] *Department of Chemistry, Women's College, Agartala, Tripura 799001, India*
[b] *Department of Forestry and Biodiversity, Tripura University, Suryamaninagar, Tripura, India*
[c] *Department of Chemistry, Netaji Subhash Mahavidyalaya, Udaipur, Tripura 799 114, India*
[d] *In Silico Drug Design Lab., Department of Pharmacy, Tripura University, Suryamaninagar, Tripura, India*
[e] *Department of Chemistry, Faculty of Science, Imam Mohammad Ibn Saud Islamic University, Riyadh 11623, Saudi Arabia*

ABSTRACT

Background: According to the International Diabetes Federation, there will be 578 million individuals worldwide with diabetes by 2030 and 700 million by 2045. One of the promising drug targets to fight diabetes is α-glucosidase (AG), and its inhibitors may be used to manage diabetes by reducing the breakdown of complex carbohydrates into simple sugars. The study aims to identify and validate potential AG inhibitors in natural sources to combat diabetes.
Methods: Computational techniques such as structure-based virtual screening and molecular dyncamic simulation were employed to predict potential AG inhibitors from compounds of *Oroxylum indicum*. Finally, in silico results were validated by *in vitro* analysis using *n*-butanol fraction of crude methanol extracts.
Results: The XP glide scores of top seven hits OI_13, OI_66, OI_16, OI_44, OI_43, OI_20, OI_78 and acarbose were −14.261, −13.475, −13.074, −13.045, −12.978, −12.659, −12.354 and −12.296 kcal/mol, respectively. These hits demonstrated excellent binding affinity towards AG, surpassing the known AG inhibitor acarbose. The MM-GBSA dG binding energies of OI_13, OI_66, and acarbose were −69.093, −62.950, and −53.055 kcal/mol, respectively. Most of the top hits were glycosides, indicating that active compounds lie in the *n*-butanol fraction of the extract. The IC_{50} value for AG inhibition by *n*-butanol fraction was 248.1 μg/ml, and for that of pure acarbose it was 89.16 μg/ml. The predicted oral absorption rate in humans for the top seven hits was low like acarbose, which favors the use of these compounds as anti-diabetes in the small intestine.
Conclusion: In summary, the study provides promising insights into the use of natural compounds derived from *O. indicum* as potential AG inhibitors to manage diabetes. However, further research, including clinical trials and pharmacological studies, would be necessary to validate their efficacy and safety before clinical use.

1. Introduction

Diabetes mellitus is a severe health issue worldwide that is a chronic metabolic illness with an intensified growth rate. Diabetes impacted 529 million people worldwide in 2021, and more than 1.31 billion are projected to be affected by 2050 (Ong, 2023). There are three main types of diabetes: type 1 diabetes (T1D), type 2 diabetes (T2D), and gestational diabetes mellitus (GDM). Most of the people (approx. 90 %) with diabetes have T2D (Saeedi et al., 2019). Diabetes-related medical expenses are increasing day to day, subsequently placing a severe financial strain

on nations and their citizens. Unlike T1D, T2D is a condition in which our body does not create enough insulin or gets resistant to insulin. Despite significant advancements in anti medications, only a limited number of drugs are clinically effective. There are six different classes of active pharmaceutical ingredients or oral anti-diabetic drugs currently available and are taken orally to treat T2D condition, namely biguanides (e.g., metformin), sulfonylureas (e.g., glimepiride), meglitinides (e.g., repaglinide), thiazolidinediones (e.g., pioglitazone), dipeptidyl peptidase IV inhibitors (e.g., sitagliptin), and α-glucosidase inhibitors (e.g., acarbose). (Feingold, 2000)). There is a strong correlation between T2D
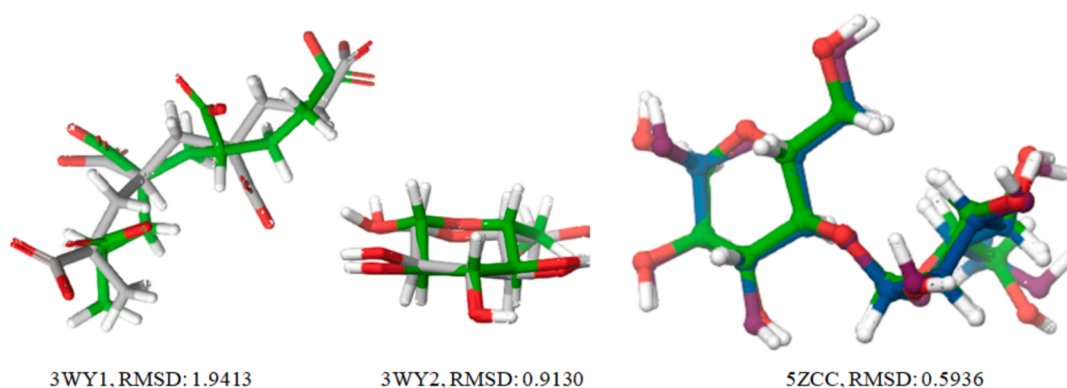
Fig. 1. Superposition of the docked co-ligands (3R,5R,7R)-octane-1,3,5,7-tetracarboxylic acid, ß-D-glucopyranose, and α-maltose on their respective crystallographic bound conformation (green) of (PDB IDs: 3WY2, 3WY1 and 5ZCC).

Table 1
XP Glide score, MM-GBSA dG$_{Bind}$, active site interacting amino acid residues of selected top seven hits and known inhibitor Acarbose.

Compound	XP Glide Score(kcal/mol)	MM-GBSA dG Bind(kcal/mol)	Interacting amino acid residues
OI_13	−14.261	−60.524	HIS-203, GLN-256(2),ASN-258 (2), MET-285, ASP-327, GLN-328 (2), THR-409
OI_16	−13.074	−35.422	TYR-63 (π-π interaction), ILE-143, ASN-258, MET-285, GLN-328, ASP-382, THR-409, ARG-411
OI_20	−12.659	−29.359	ASP-60, HIE-103, ARG-197, ASP-199, GLN-256, ASN-258, THR-409
OI_43	−12.978	−19.022	HIE-103, PHE-144 (π-π interaction), ASP-199(2), HIS-203, GLN-256, ASN-258, ARG-411
OI_44	−13.045	−37.071	ARG-44, ASP-60, HIE-103, ASP-199, ASN-256, HIE-326, ASP-327 (3)
OI_66	−13.475	−43.908	ILE-143, GLN-256, ASN-256, PHE-282 (3)(π-π interaction), ASP-327 (2), GLN-328
OI_78	−12.354	−35.659	ASP-60, HIE-103(2), ARG-197, ASP-199, HIS-203, GLN-256, ASN-258, ASP-327, ARG-411
Acarbose	−12.296	−42.832	ASP-60, ASP-199, ASN-258, PHE-282, ASP-327, GLN-328

and a number of ocular illnesses like retinopathy, glaucoma, placental microvascular abnormalities in gestational period (Chen et al., 2023; Liang et al., 2023) etc. Drugs are also available to address issues associated with diabetes; andrographolide, a potent medication to prevent and treat calcific aortic valve disease related to diabetes, which reduces calcification by interfering with H3Kla via p300 (Wang et al., 2024).

Initially, an enzyme like amylase is responsible for breaking down complex carbohydrates into smaller fragments such as oligosaccharides and disaccharides. However, these fragments must first be broken down into glucose molecules so that they can enter the blood stream and be utilized as fuel. The enzyme α-glucosidase plays an important role in this conversion. One of the therapeutic approaches is to decrease postprandial hyperglycemia by retarding the absorption of glucose by inhibition of carbohydrate-hydrolyzing enzymes, such as α-amylase and α–glucosidase. α-Glucosidase inhibitors reduce this enzyme's activity and delay the digestion and absorption of carbohydrates in the small intestine. Inhibition of α-glucosidase causes a slower and more consistent release of glucose into the blood stream, which helps to minimize blood sugar concentration after meals. If α-glucosidase activity is inhibited, the glucose conversion rate has to be slower and will produce

limited glucose molecules at a time. FDA-approved three synthetic drugs, acarbose, miglitol, and voglibose are well-known α-Glucosidase inhibitors to treat T2D to date (Junge et al., 1996, Rydén et al., 2013). However, prolonged use of these medicaments was reported with several adverse effects like vomiting, liver disorders, flatulence, abdominal discomfort, hypoglycemia, urinary tract infection, etc., in patients. In this context, it is desirable to identify potential novel synthetic or natural α-glucosidase inhibitors effective with minimum side effects. Several researchers have recently developed new synthetic α-glucosidase inhibitors and predicted their inhibitory potential (Gul et al., 2024; Khan et al., 2023; Alam et al., 2022). There are several other strategies to treat diabetes and diabetes-related complications. A mitophagy regulation mechanism may be a potential target for the development of lipotoxicity-related T2D. Treatment of nephropathy related to diabetes in the future could involve restoring glomerular filtration barrier damage by manipulation of adenosine monophosphate-activated protein kinase activity (Yang et al., 2021, Li et al., 2023). The prevalence of T2D in Europe was lower than the global average, but substantial from T2D, reflecting the diversity of regions. In order to lower the risk of T2D, other than medication, enhance healthcare systems, decrease the waist circumference and body mass index, provide affordable treatment, region-specific interventions are required to address the rising incidence of both T1D and T2D (Ling *et al.*, 2023, Zhou et al., 2023). To reduce diabetes and diabetes-related complications, continuous monitoring is required along with the use of highly sensitive detecting component, medication and lifestyle modification. Another important aspect is to increase the efficacy of current drugs like metformin (Zhou et al., 2022, Xiao et al., 2016). It is observed that over 60–80 % of the world's population still relies on conventional medicines to treat common ailments (Libman et al., 2006). Natural substances are the basis of novel therapeutic lead molecules with minimal side effects, and the use of natural bioactive compounds is the replacement therapy for our contemporary therapeutic developments (Chen et al., 2023; Su et al., 2023). Edible natural products may be a valuable source of medication for so many ailments with lower toxicity and side effects (Dirir et al., 2022). Bioactive natural substances available in edible plants have recently emerged as effective methods against several diseases. The present work aims to predict and identify the potential α-glucosidase inhibitors from the fruits of an edible plant source using a rational drug design approach and validate the theoretical study simultaneously with laboratory experiments. The selection of plant *O. indicum* (L.) Kurz, for our study, was considered based on its traditional knowledge. It is a tree that is used as a traditional medicine for the prevention and treatment of a wide range of illnesses, including jaundice, arthritic and rheumatic conditions, gastric ulcers, tumors, respiratory illnesses, diabetes, diarrhea, and dysentery (Dinda et al., 2015).

Unlike our present study, Bhatia *et al.* investigated and showed potent α-glucosidase inhibitory activity of methanolic extract of *Cornus*
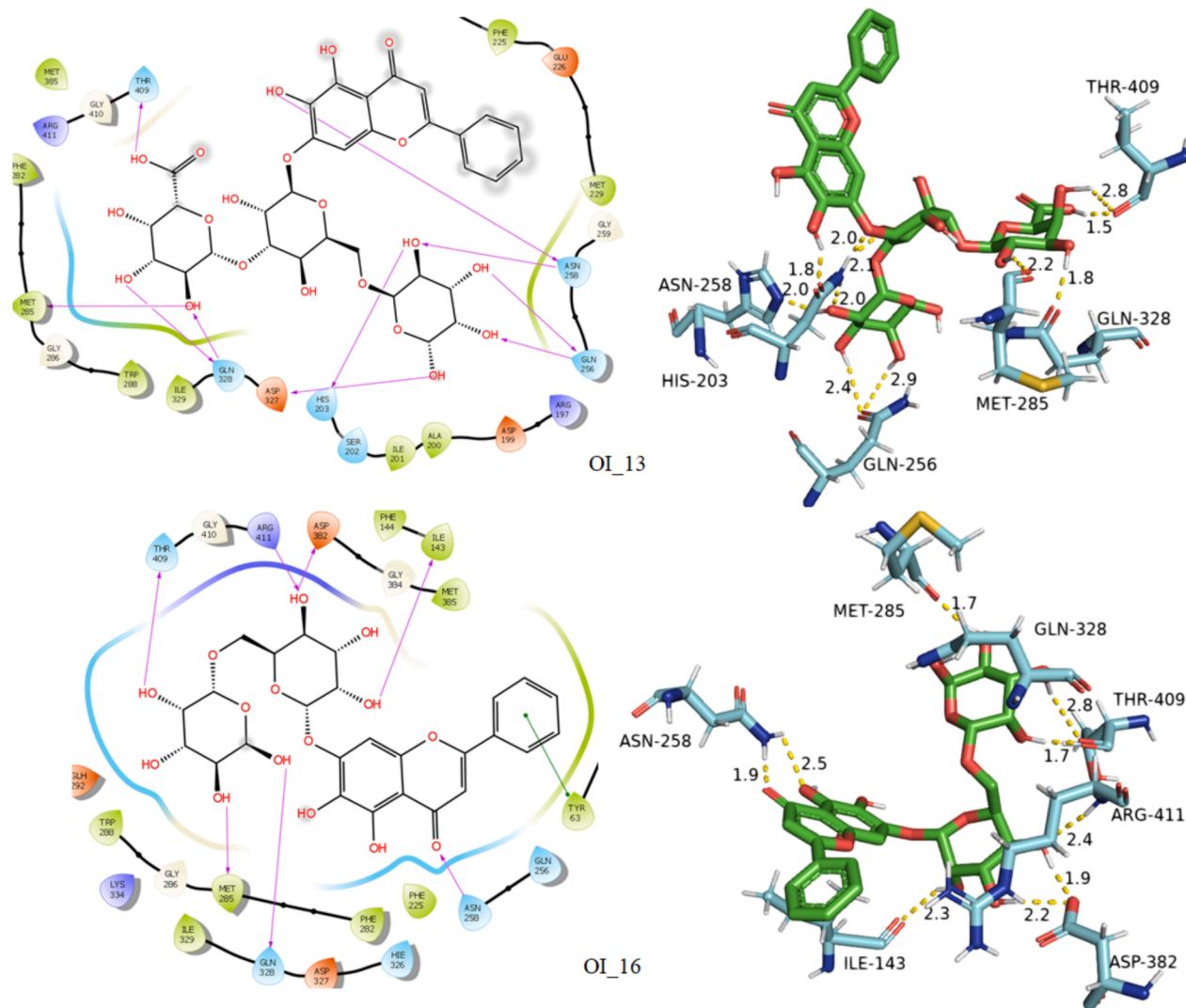
Fig. 2. 2D and 3D protein–ligand interaction diagrams of selected hits and standard α-glucosidase inhibitor acarbose (OI_13, OI_16, OI_20, OI_43, OI_44, OI_66, OI_78 and Acarbose).

capitata leaves (Bhatia et al., 2019). Whereas Libman *et al.* and Chhetri *et al.,* studied separately to evaluate the anti-diabetes activity of *O. indicum* root and bark, respectively, to validate its traditional knowledge (Libman et al., 2006, Chhetri et al., 2005). Further, Swargiary *et al.* identified a few selected volatile compounds from leaf extracts of *O. indicum* using GC–MS analytical techniques and studied α-glucosidase inhibitory activity of the same (Swargiary & Daimari, 2020). Though systematic investigations on natural products have been going on for several decades using modern, sophisticated instruments, only very few bioactive molecules were isolated and reported from this plant. All these facts motivate us to investigate further to predict and identify bioactive compounds of *O. indicum* as anti-diabetic potential and to validate the traditional use of *O. indicum* for several decades. For this, the compounds of *O. indicum* were retrieved from literature and predicted the α-glucosidase inhibitory potential using structure-based virtual screening. However, the stability of potential protein–ligand complexes was revealed using MD simulation. Finally, the selective fraction of the plant extract was evaluated for α-glucosidase inhibitory activity based on in silico study results to validate the computational findings.

2. Materials and methods

2.1. Dataset

The compounds of *O. indicum* were retrieved from the literature (Dinda et al., 2015, Swargiary *et al.,* 2020, Deka et al., 2013). All 91 structures (Figure S1) were drawn using ChemDraw Professional 15.1 and saved in sdf format. The X-ray crystal structure of α-glucosidases, PDB ID: 3WY1, Resolution: 2.15 Å (Shen et al., 2015), PDB ID: 3WY2, Resolution: 1.47 Å (Shen et al., 2015), and PDB ID: 5ZCC, Resolution: 1. 70 Å (Kato et al., 2018, Auiewiriyanukul et al., 2018) were retrieved from Research Collaboratory for Structural Bioinformatics (RCSB.) Protein Data Bank (https://www.rcsb.org/). All the computational works were carried out using Dell Inc., System Model: Precision 5820 Tower, Processor: Intel(R) Xeon(R) W-2245 CPU @ 3.90 GHz (16 CPUs), ~3.9 GHz, OS: Ubuntu 22.04.1 LTS, 64-Bit.

2.2. Ligand preparation

The initial step in the molecular docking process was ligand preparation. All the structures were imported into Maestro (Schrödinger, 2021), and geometric refinement with the Ligprep module (Schrödinger,
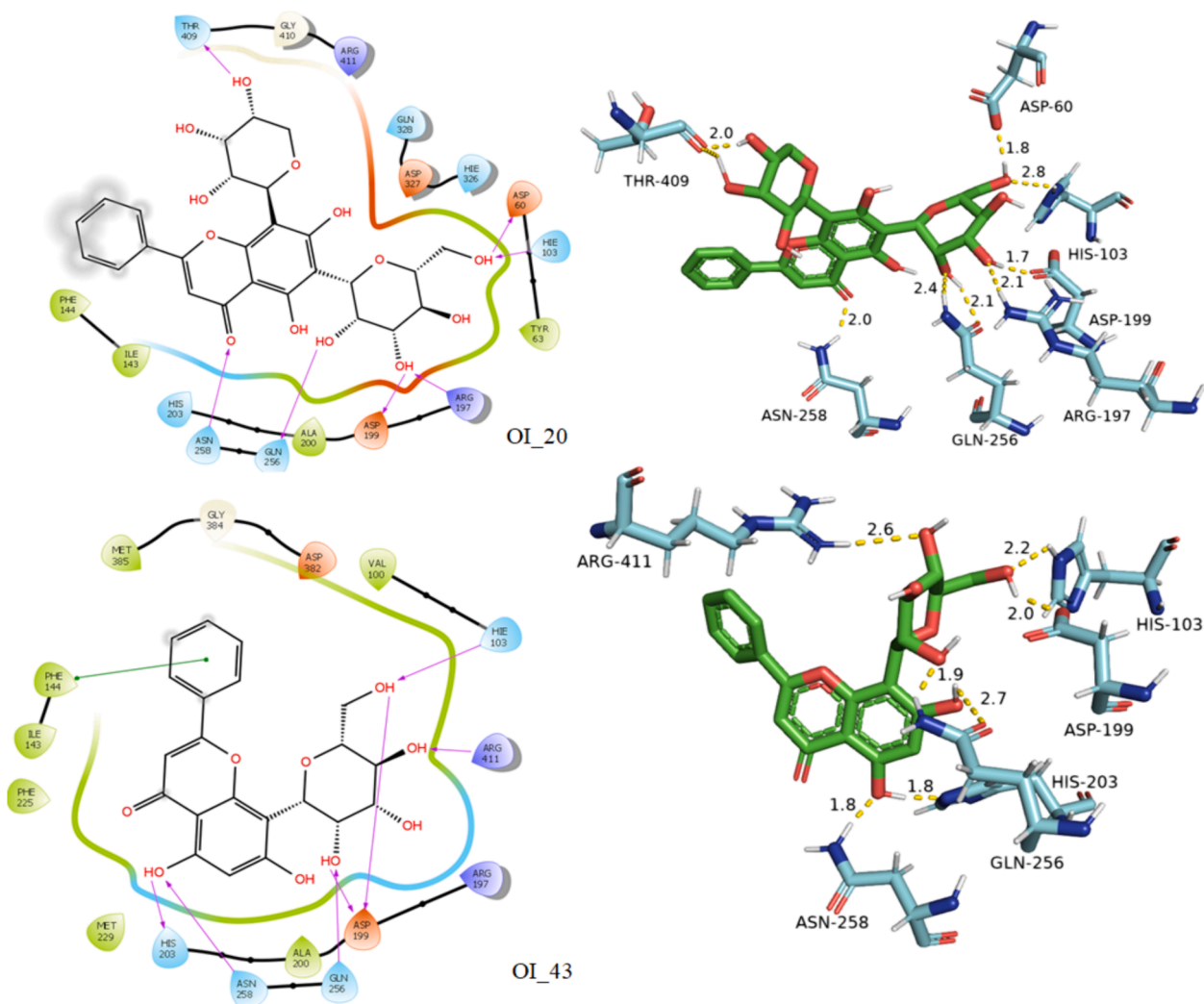
Fig. 2. (*continued*).

2021) LigPrep creates a single, low-energy, 3D structure with the proper
chiralities for each properly provided input structure. In this stage, the
original states of ionization and chiralities were determined from the 3D
structure. The conformers were then all minimized using the OPLS_2005
force field.

2.3. Preparation of target protein and grid generation

The X-ray crystal structures of α-glucosidase were downloaded from
the RCSB protein databank (https://www.rcsb.org/). All the proteins
(PDB ID: 3WY2, 5ZCC, and 3WY1) were imported into Maestro. All the
proteins were prepared using the default option of the Protein Prepa-
ration Wizard of Schrodinger. The receptor grid was generated using the
prepared protein α-glucosidase by selecting their respective co-ligand,
setting the grid dimension to 15.0 Å from the co-ligand's center. This
receptor grid was used for the virtual screening database using Glide
(Friesner et al., 2006, Halgren et al., 2004, Friesner et al., 2004).

2.4. Validation of docking

The accuracy of the docking protocol was calculated by measuring
the root mean square deviation (RMSD). The RMSD was calculated by
superimposing the docked pose of the co-ligand on its original crystal-
lographic bound conformation. The lower value of RMSD indicates
higher docking accuracy, and RMSD values less than 2.0 Å, depending

on ligand size, are considered to have been performed successfully
(Hevener et al., 2009). Amongst the several α-glucosidase crystal
structures, the lowest RMSD PDB ID was selected for virtual screening
studies.

2.5. Virtual screening (VS) of in-house database

The structure-based virtual screening (VS) of compounds of
O. indicum against α-glucosidase (PDB ID: 5ZCC) was performed using
the virtual screening tool of Glide. In the workflow, the filtered hits were
submitted to HTVS-based molecular docking. The top 60 % of the hits
resulting from HTVS were submitted to SP docking. Again, the top 60 %
of the hits obtained from SP were then subjected to XP docking, and 80
% of output molecules were considered for score prediction. Then, the
output molecules were subjected to MM-GBSA dG Bind = Complex −
Receptor − Ligand energy calculation (Li et al., 2011). The workflow of
the present study is shown in Fig. 10.

2.6. MD with Desmond simulation package

Molecular dynamics simulation is the simplest and most widely used
method for assessing the stability of the protein–ligand complex. After
molecular docking, the binding sites for α-glucosidase were subjected to
MD simulations using the Desmond package. To determine the stability
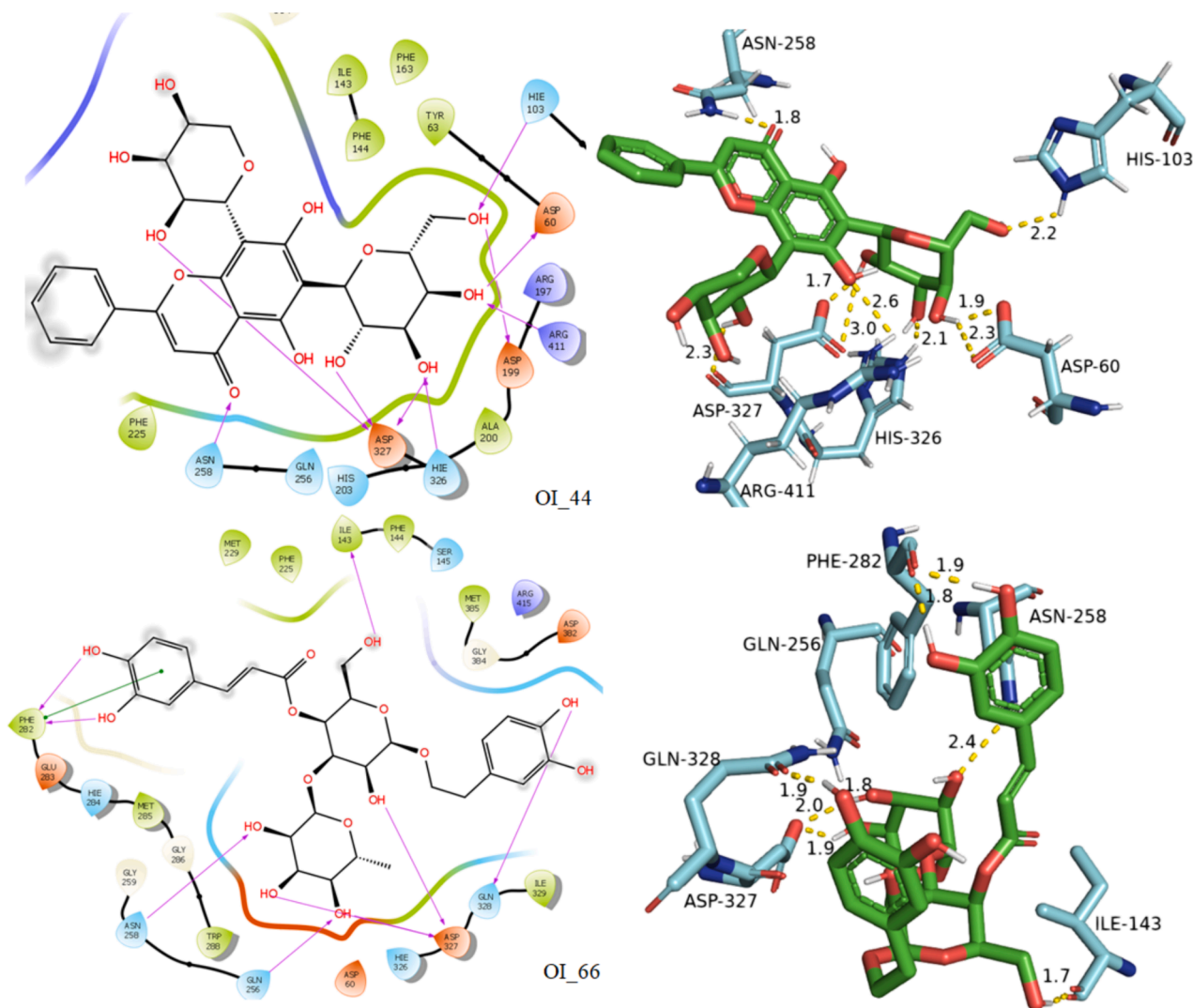of the protein backbone in the docked complex, a 100 ns molecular

Fig. 2. (*continued*).

dynamics simulation experiment was performed using the Desmond program of Schrodinger, an explicit solvent MD package, and a fixed OPLS_2005 force field (Schrödinger-Desmond Shaw D. E. Research, 2021, Kevin et al., 2006). The best-docked pose for each protein and ligand have been saved separately in pdb format and then imported once again into PyMOL (Lilkova et al., 2015). The protein–ligand complexes were imported in PyMOL, and then the complex was exported in pdb format. The OPLS force field's default settings were used to parameterize the ligands in the Desmond model. The protein–ligand complexes were fixed in an orthorhombic periodic box that was soaked in solvent, with a minimum gap between the protein atoms and the box borders of 10.0 Å. The solvent was applied using a single-point charge (SPC) water model (Mark & Nilsson, 2001). The charge of the system was neutralized by the addition of 0.15 M NaCl, Na$^+$, and Cl$^-$ counterions. Using the Desmond System Builder panel, the salt concentration was adjusted to match the physiological system (Jorgensen et al., 1996). To relax the system into a local energy minimization, a minimization task was carried out. Then, using the OPLS_2005 force field parameter, this model system was put into MD simulation stages. The simulation was run using the NPT ensemble (Isothermal-Isobaric ensemble, constant temperature, constant pressure, constant number of particles) at 300.0 K temperature and 1.013 bars pressure with the relaxation settings left at default (Kalibaeva et al., 2003). The temperature was controlled using the Noose-Hover chain thermostat algorithm, while the pressure was controlled using

the Martyna-Tobias-Klein barostatal method (Martyna, 1994). A cut-off of 9.0 was utilized for nonbonded interactions, the Particle Mesh Ewald (PME) approach was used for long-range electrostatic interaction, and the remainder of the parameters were left at their default values (Toukmaji et al., 1996). The behavior and interactions between the ligands and proteins were examined using the Simulation Interaction Diagram (SID) tool. Root Mean Square Deviation (RMSD) and Root Mean Square Fluctuation (RMSF) were chosen in the analysis type after loading the cms file to create the aforementioned figures.

2.7. ADME prediction of selected inhibitors

Prediction of absorption, distribution, metabolism, and excretion (ADME) are crucial components in establishing drug pharmacokinetics. ADME prediction can help to discover compounds with advantageous ADME properties early in the drug discovery process, reducing the time and cost to manufacture a novel treatment by half. The ADME properties of selected inhibitors were predicted by QikPro (Schrödinger, QikProp, 2021). QikProp provides ranges for comparing specific ADME properties with 95 % of recognized drugs.

2.8. Collection of plant materials

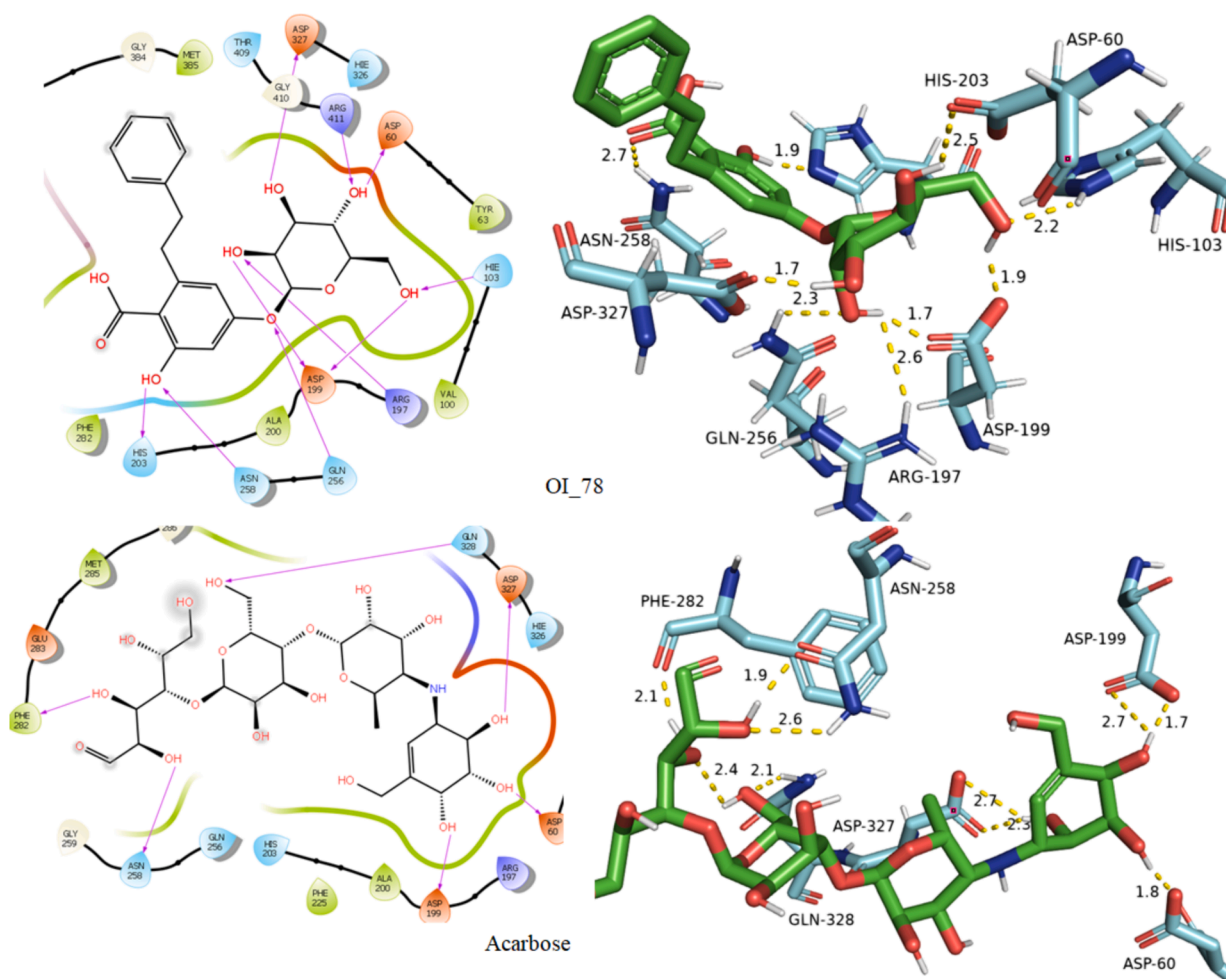The fresh bark of *O. indicum* was obtained from the Tripura

Fig. 2. (*continued*).

University campus, Tripura, India. All necessary permissions were obtained for plant collection through the Department of Forestry and Biodiversity, Tripura University. The research also complies with all applicable regional and national regulations. The sample was collected following the guidelines of IUCN and SITES (https://cites.org/eng/app/index.php).

2.9. Identification and preparation of plant materials

A certified botanist and taxonomist of the Department of Botany, Tripura University, Tripura, India, systematically identified and authenticated the plant species. A voucher specimen (Call NoTUH-4407) of the *O. indicum* flowering plant was deposited in the Department of Botany, Tripura University, Tripura, India. The entire plant bark was scrubbed clean with tap water and then left to dry naturally without exposure to sunlight at room temperature. The dried bark was cut into tiny pieces and shaded-dried for 2–3 weeks.

2.10. Preparation of crude extracts

The dried material was initially crushed into fine powder, and 500 gm of powdered bark was subjected to cold maceration sequentially in an extracting jar with petroleum ether (1:3 w/v) for two days and then with 1500 mL of methanol. The prepared solution was kept at room temperature for 48 h, followed by filtration using Whatman filter paper-1. Afterward, the filtrate was concentrated by evaporating methanol solvent in a rotary evaporator at 40 °C to obtain crude extract. The concentrated solution was then dried at 4 °C to eliminate excess solvent.

The procedure was repeated three times to collect the crude residue. The dried crude residue was then dissolved in 200 ml of deionized water, and the solvent extraction procedure was used to fractionate it. The aqueous extract was mixed with ethyl acetate (1:1) and separated using a separating funnel, followed by *n*-butanol. The *n*-butanol fraction was stored at −20 °C for further use in in-vitro α-glucosidase inhibitory assay.

2.11. In-vitro α-glucosidase inhibitory assay

The plant extract was evaluated for α-glucosidase inhibitory activity according to the method given by Pistia-Brueggeman and Hollingsworth (Pistia-Brueggeman and Hollingsworth, 2001) with minor modifications. Plant extract 100 µl (*n*-butanol fraction) at varying concentrations (25–500 µg/mL) was incubated with 20 µL of the α-glucosidase (5 U/ml) for 25 min at 37 °C with an additional 250 µL of 0.1 M phosphate buffer (pH 6.8). After 25 min, the reaction was started with the addition of 40 µL of 1 M pNPG as substrate, and the mixture was incubated for 45 min at 37 °C. The reaction was terminated with the addition of 0.1 N of Na_2CO_3 (100 µL), and final absorbance (Abs) was measured at 405 nm using a spectrophotometer. The standard compound acarbose was used as a positive control at varying concentrations (25–500 µg/mL). Enzyme activity was measured and calculated using the following formula:

% inhibition of α-glucosidase = (Abs_{Blank} − Abs_{Sample}) / (Abs_{Blank}) × 100

Each unit of enzyme can be defined as the amount of enzyme (α-glucosidase) involved in the formation of one µmol of the end product (p-Nitrophenol) from the substrate (p-nitrophenyl-α-D-
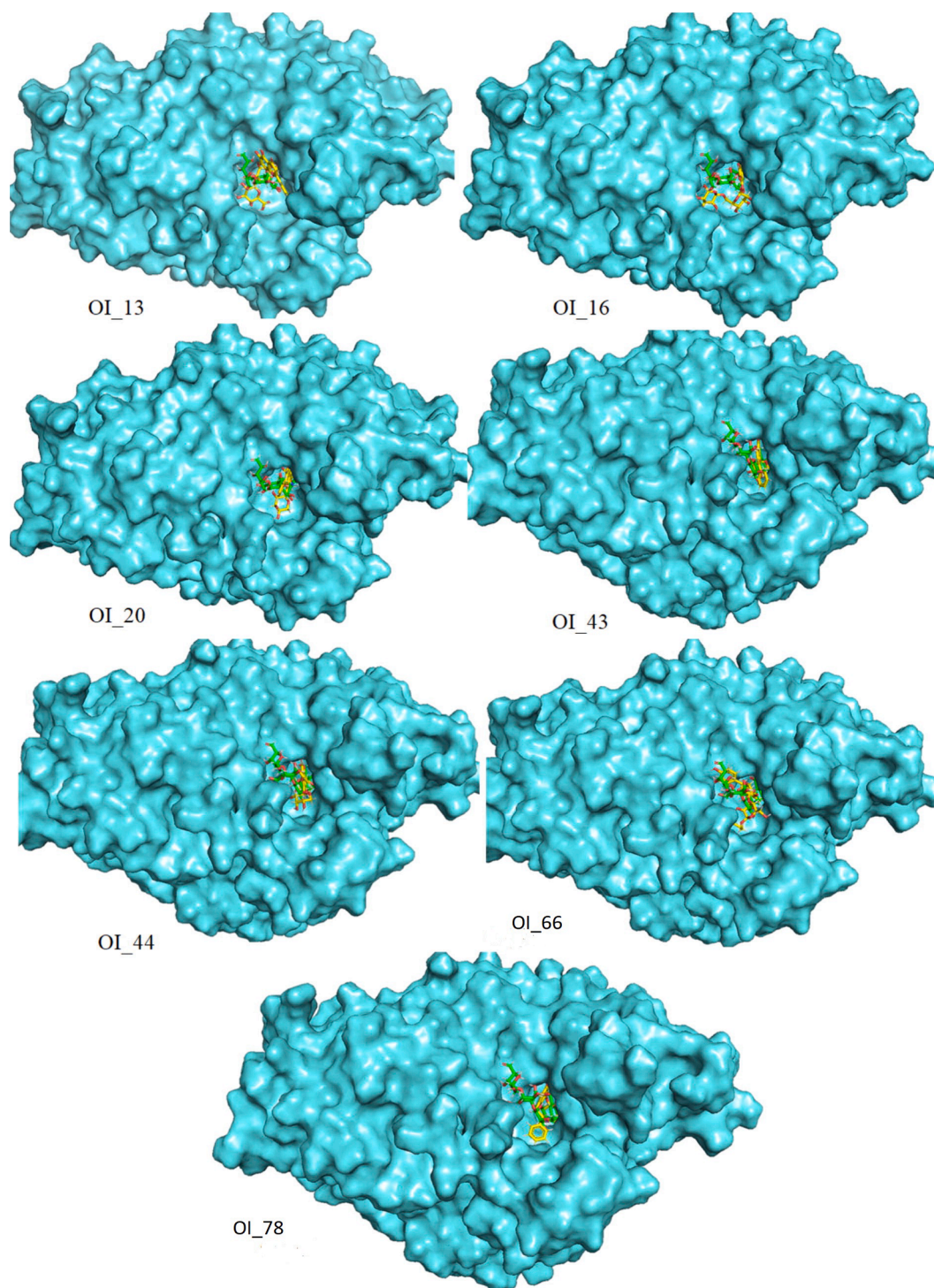
Fig. 3. The binding pose in 3D space of selected hits OI_13, OI_16, OI_20, OI_43, OI_44, OI_66, OI_78 in the active site of α-glucosidase.

glucopyranoside) per minute. IC_{50} (concentration required to inhibit 50 % of the enzyme activity) was calculated using regression a equation obtained through plotting concentration in the range 25–500 μg/mL (x-axis) and percentage inhibition (y-axis) for *n*-butanol fraction as well as standard. The enzymes and chemicals were procured from Sisco Research Laboratories Pvt. Ltd. (SRL) − India. The purity of n-butanol, p-Nitrophenyl-ß-D-Glucuronide (pNPG) extra pure, and Na_2CO_3, was 99 %, 99 %, and 99.5 %, respectively.

3. Results

In the present study, structure-based virtual screening of a library of 91 compounds (**Figure S1**) of *O. indicum* was carried out to identify potential α-glucosidase inhibitors. For structure-based VS, validation of the docking protocol was crucial, and it was measured using root mean square deviation (RMSD). The RMSD values of docked co-ligands of PDB IDs of α-glucosidase: 3WY2, 3WY1, and 5ZCC were 1.9413, 0.9130, 0.5936 Å, respectively, when superimposed on their respective original crystallographic bound conformation (green) are shown in Fig. 1.

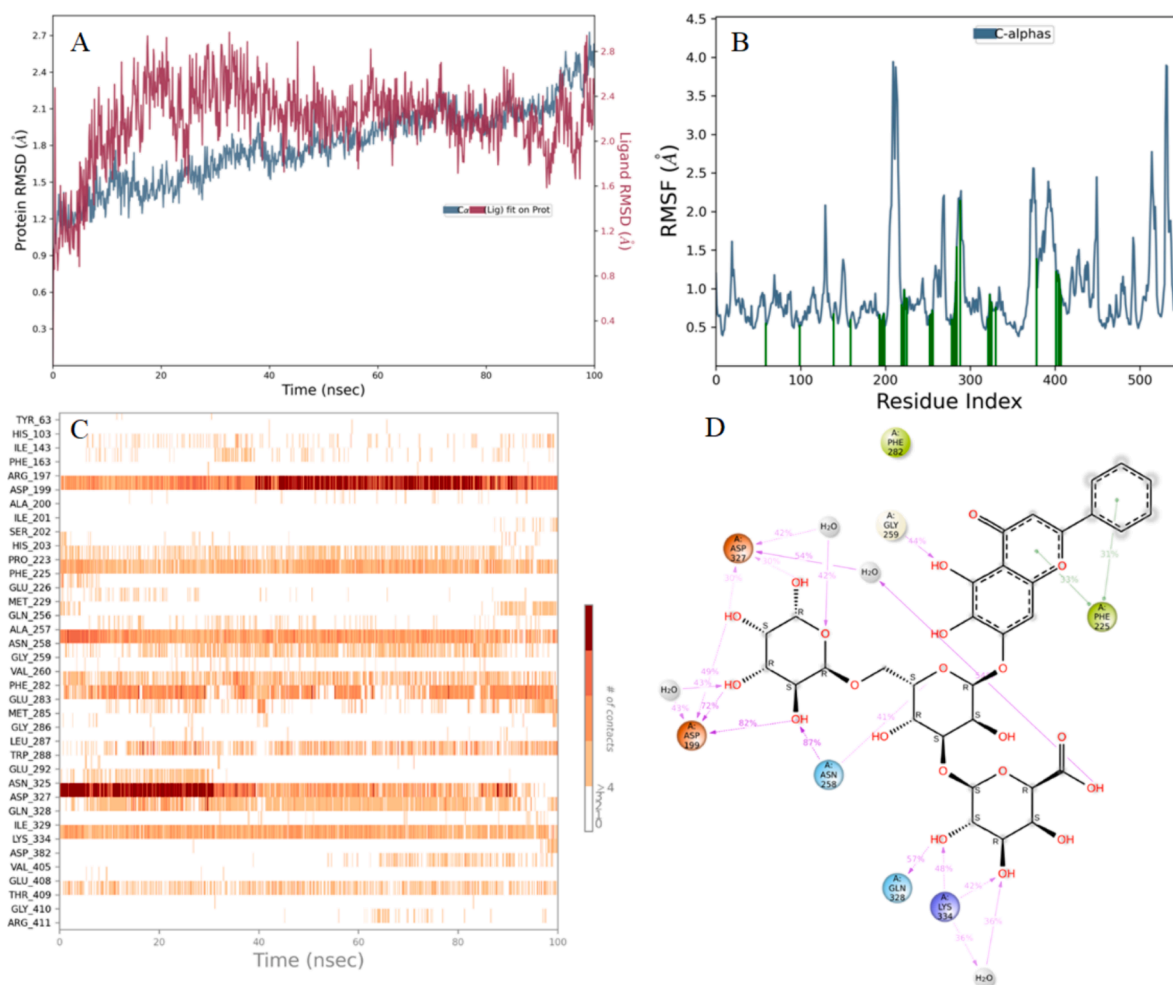The virtual screening (VS) of all the prepared molecules of the library

Fig. 4. Protein-ligand (OI_13) RMSD. Cα (violet) and Lig-fit (purple) (A), protein–ligand (OI_13) RMSF change (B), timeline representation of Protein-Ligand contacts (C), 2D ligand interaction diagram and binding pose of ligands OI_13 (D), with active site residues during 100 ns simulation.

resulted in seven hits having XP glide score superior to the standard α-glucosidase inhibitor acarbose (XP Glide score: −12.296 kcal/mol). The XP Glide score of top seven hits OI_13, OI_16, OI_20, OI_43, OI_44, OI_66 and OI_78 were −14.261, −13.074, −12.659, −12.978, −13.045, −13.475, −12.354 kcal/mol, respectively. Table 1 summarizes the XP Glide score of top seven selected hits along with active site interacting amino acid residues. The 2D and 3D protein–ligand visual representations of the selected top seven hits are presented in Fig. 2. The XP Glide score and MM-GBSA dG binding energy of top hits exported from hits VS result are shown in Figure S2. The MM-GBSA dG bind energy predicted from VS of OI_13, OI_16, OI_20, OI_43, OI_44, OI_66, OI_78 and Acarbose were −60.524, −35.422, −29.359, −19.022, −37.071, −43.908, −35.659 and −42.832 kcal/mol, respectively. The MM-GBSA dG binding energy predicted from VS of the selected top hits is demonstrated in Table 1. Detailed analysis of each molecule in 3D surface view orientation within the α-glucosidase active site cavity is shown in Fig. 3**.**

The 100 ns molecular dynamics simulation further assessed the stability of protein–ligand complexes and the interaction properties of selected hits, OI_13, OI_66, OI_78, and standard α-glucosidase inhibitor acarbose with the α-glucosidase were monitored simultaneously. The calculation was performed for each frame in the simulation trajectory to evaluate the stability of complexes over time. The RMSD, RMSF, and ligands atom interactions with protein residues are depicted in Figs. 4–7. The average range RMSD and RMSF of protein–ligand (OI_13, OI_66, & OI_78) complexes ranged from 1.882–2.633 Å and 1.896–2.478 Å, respectively. The average range of RMSD and RMSF of protein-acarbose

complex were 2.414 Å and 1.849 Å, respectively. The maximum, minimum, and average RMSD and RMSF results of protein–ligand complexes of OI_13-5ZCC, OI_66-5ZCC, and OI_78-5ZCC are illustrated in Table 2.

The interacting amino acid residues of α-glucosidase with acarbose during simulation time were identified as HIS-103, ASP-199, ASN-258, PHE-282, GLU-283, TRP-288, HIS-326, ASP-327, and ARG-411. In case of OI_13, the interacting amino acid residues were observed as ASP-199, PHE-225, ASN-258, GLY-259, ASP-327, GLN-328, and LYS-334. The interacting amino acid residues of the enzyme with OI_66 were found as ASP-199, ASN-258, GLY-259, GLU-283, ASN-325, and ASP-327. Similarly, the interacting amino acid residues of α-glucosidase with OI_78 were identified as ASP-60, ASP-199, HIS-203, ASP-289, ARG-411, and ARG-415.

The MM-GBSA dG bind of complexes OI_13-5ZCC, OI_66-5ZCC, OI_78-5ZCC, and acarbose were analyzed to determine the affinity of the ligand towards the receptor. The predicted binding energies and contributing factors of protein–ligand complexes are shown in Table 3. The binding free energies (ΔG_{bind}) of hits OI_13, OI_66, OI_78, and acarbose were −69.093, −62.950, −38.982, and −53.055 kcal/mol, respectively, for the receptor 5ZCC. A more negative value shows stronger binding free energy.

The *n*-butanol fraction of crude extract of *O. indicum* bark was selected for *in vitro* activity study and showed significant inhibitory activity with an IC$_{50}$ value of 248.1 μg/ml on α-glucosidase comparable to standard acarbose (IC$_{50}$ 89.16 μg/ml). The activity of the *n*-butanol fraction and standard inhibitor are shown in Table 4 and Figs. 8 & 9.
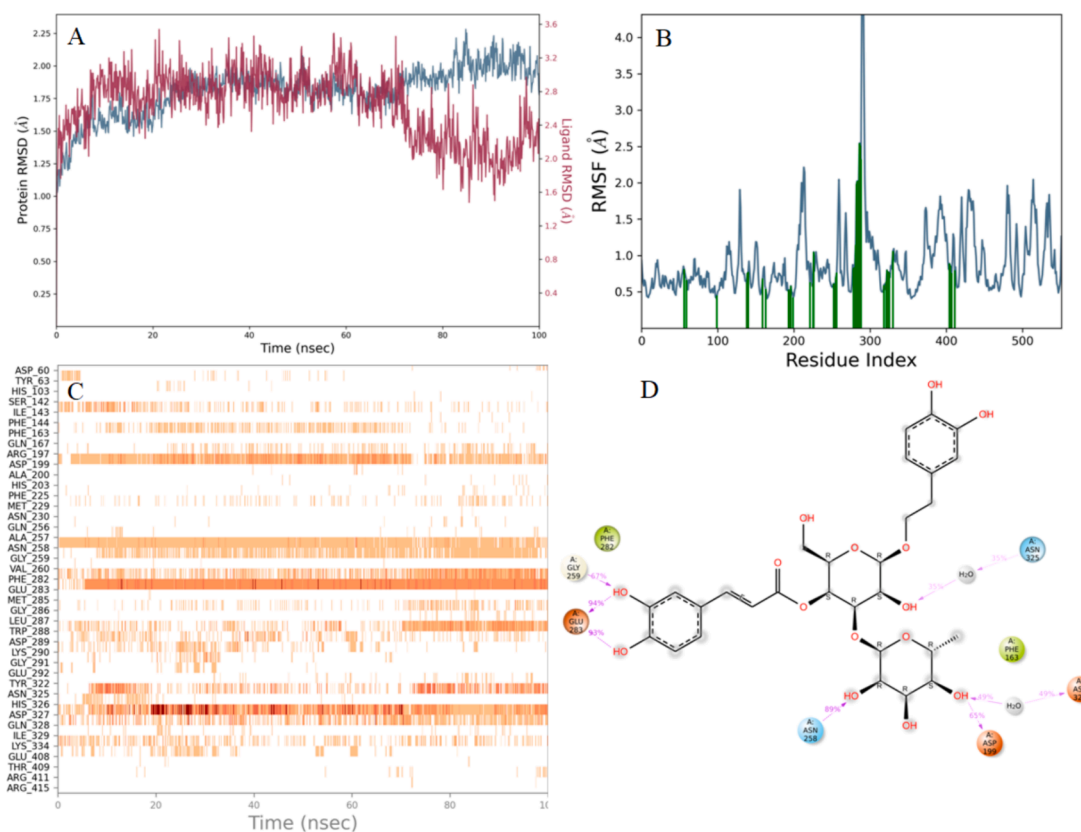
Fig. 5. Protein-ligand (OI_66) RMSD. Cα (violet) and Lig-fit (purple) (A), protein–ligand (OI_66) RMSF change (B), timeline representation of Protein-Ligand contacts (C), 2D ligand interaction diagram and binding pose of ligands OI_66 (D), with active site residues during 100 ns simulation.

Fig. 6. Protein-ligand (OI_78) RMSD. Cα (violet) and Lig-fit (purple) (A), protein–ligand (OI_78) RMSF change (B), timeline representation of Protein-Ligand contacts (C), 2D ligand interaction diagram and binding pose of ligands OI_78 (D), with active site residues during 100 ns simulation.
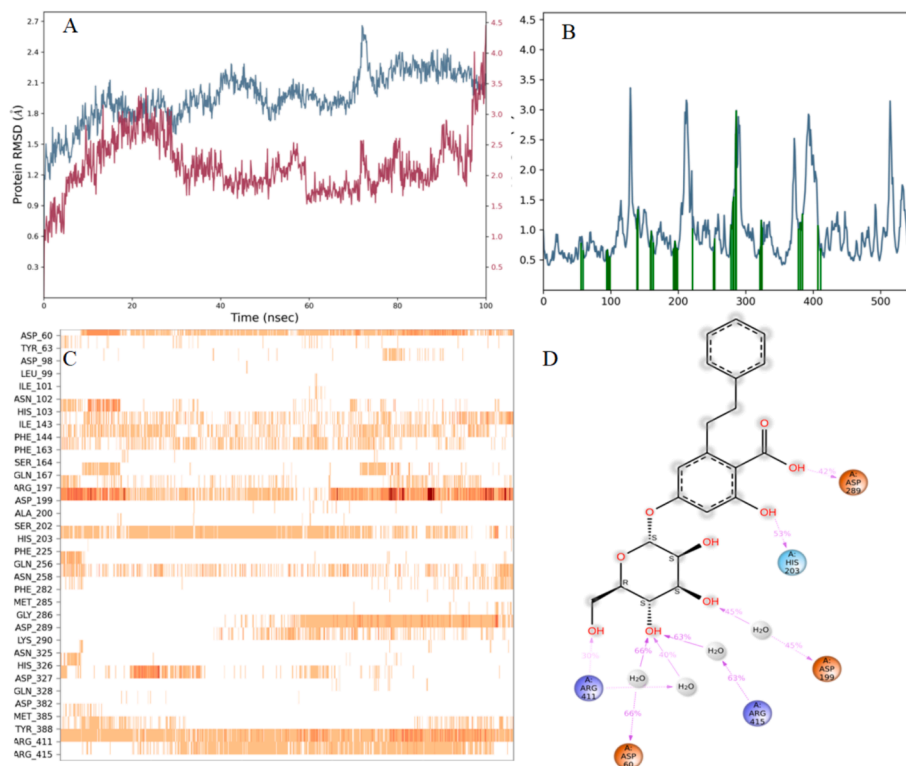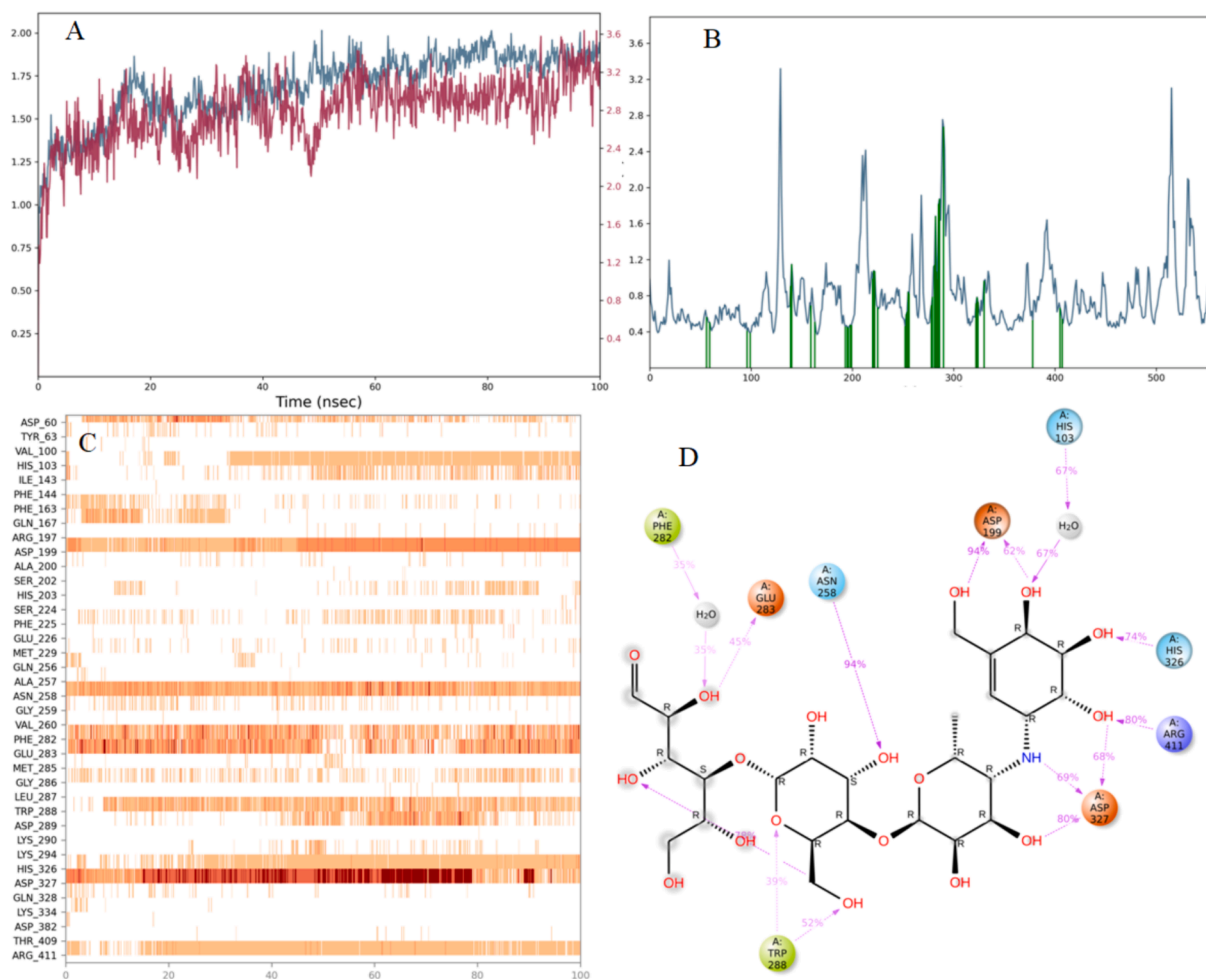
Fig. 7. Protein-ligand (DB00284) RMSD. Cα (violet) and Lig-fit (purple) (A), protein–ligand (Acarbose) RMSF change (B), timeline representation of Protein-Ligand contacts (C), 2D ligand interaction diagram and binding pose of ligands DB00284 (D), with active site residues during 100 ns simulation.

Table 2
RMSD and RMSF of selected protein–ligand complexes.

Name of complex	RMSD analysis (Å)			RMSF analysis (Å)		
	Minimum	Maximum	Average	Minimum	Maximum	Average
OI_13-5ZCC Complex	0.824	2.941	1.882	0.392	3.743	2.067
OI_66-5ZCC Complex	1.764	3.493	2.628	0.418	4.538	2.478
OI_78-5ZCC Complex	0.817	4.449	2.633	0.431	3.361	1.896
Acarbose −5ZCC Complex	1.191	3.638	2.414	0.381	3.318	1.849

Table 3
The MM-GBSA binding free energy, coulombic free energy, lipophilic interaction free energy, van der Waals free energy (kcal/mol).

Protein-Ligand complex	MMGBSA ΔG_{bind}	MMGBSA $\Delta G_{bind\ coulomb}$	MMGBSA $\Delta G_{bind\ lipo}$	MMGBSA $\Delta G_{bind\ vdW}$
OI_13-5ZCC	−69.093	−46.261	−25.189	−66.145
OI_66-5ZCC	−62.950	−37.765	−22.273	−59.279
OI_78-5ZCC	−38.982	−22.842	−17.047	−41.394
Acarbose-5ZCC	−53.055	−43.794	−21.103	−50.910

These results validate the in-silico findings of this study. Though the *n*-butanol fraction still contains a variety of compounds, the outcome of this study is highly encouraging and impressive compared to the pure compound acarbose.

The ADME properties of the chosen hits and known inhibitor

Table 4
α-glucosidase inhibitory activity of *n*-butanol fraction of *Oroxylum indicum* and Acarbose (standard drug).

Sample	Percentage α-glucosidase inhibition					IC_{50} (μg/ml)
	25 μg/ml	50 μg/ml	100 μg/ml	300 μg/ml	500 μg/ml	
n-butanol fraction	6.79 ± 0.52	21.09 ± 0.44	37.7 ± 0.86	67.94 ± 0.55	85.9 ± 0.79	248.1
Acarbose	31.13 ± 0.56	43.67 ± 0.17	57.21 ± 0.52	93.26 ± 0.99	98.18 ± 0.63	89.16

Values are mean ± SE of three parallel measurements; P value < 0.0001, and results statistically significant.
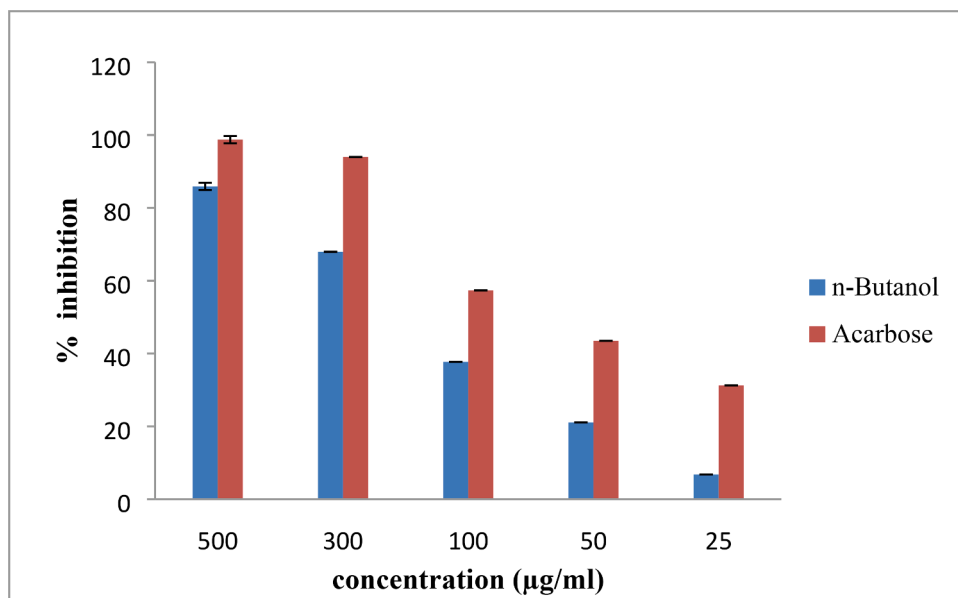
Fig. 8. The percentage of inhibition of α-glucosidase by *n*-butanol fraction of *O. indicum* and acarbose.
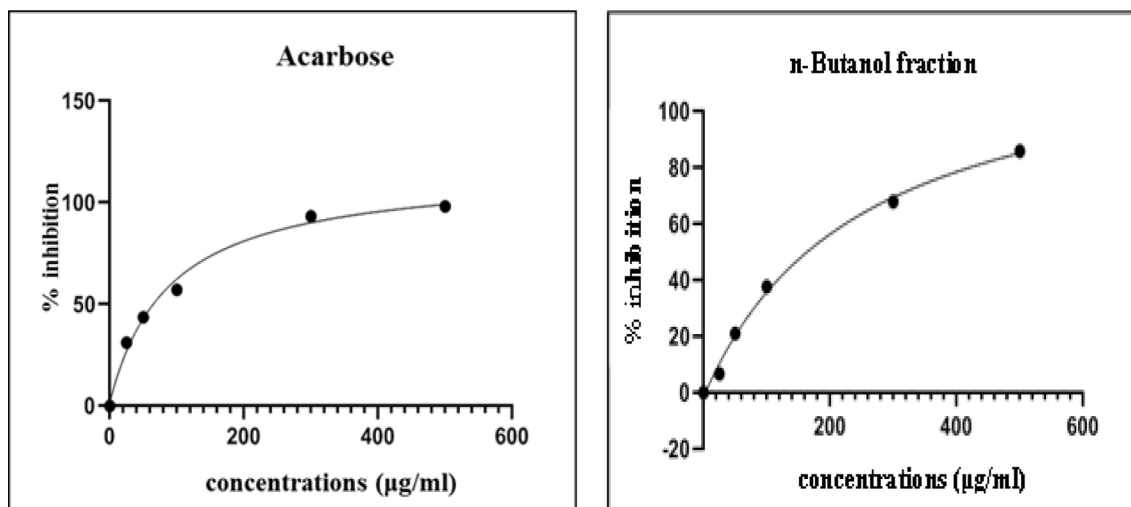

Fig. 9. Dose-response curve of acarbose and *n*-butanol fraction.

acarbose, as predicted by QikProp, are listed in **supplementary Table S1**. The human oral absorptions of compounds OI_13, OI_16, OI_20, OI_43, OI_44, OI_66, OI_78, and acarbose are 1, 1, 1, 2, 1, 1, 2, 1, and 1, respectively. The human oral absorption of compounds OI_13, OI_16, OI_20, OI_44, OI_66, and acarbose are 1, indicating that, like known inhibitors, the human oral absorption of these compounds was poor, which is excellent. The human oral absorption of OI_44 and OI_78 was 2, indicating that these compounds' absorption was medium. The percentage of human oral absorption of compounds OI_13, OI_16, OI_20, OI_44, OI_66, and acarbose were zero, which indicates that the percentage of human oral absorption of these compounds was very poor. The percentage of human oral absorption of compounds OI_43 and OI_78 were 38.39 and 27.27, respectively.

4. Discussion

The RMSD values less than 2.0 Å are considered to have performed docking protocol has good reproducibility (Hevener et al., 2009). The lower the value of RMSD, the higher the docking accuracy; therefore, 5ZCC was considered a superior protein for virtual screening.

The docking score of the selected seven hits is much higher than that of the docking score of the known inhibitor acarbose. The compound OI_13 interacted with active site amino acid residues HIS-203, GLN-256 (2), ASN-258(2), MET-285, ASP-327, GLN-328(2), THR-409. The residues ASN-258 and GLN-328 were common to known inhibitor acarbose. The compound OI_16 interacts with TYR-63 (π-π interaction), ILE-143, ASN-258, MET-285, GLN-328, ASP-382, ARG-411, THR-409 out of these ASN-258 and GLN-328 were common to known inhibitor acarbose.

The MM-GBSA dG binding energy of hit OI_13 was highest, and that of OI_43 was lowest. The molecular docking score and MM-GBSA dG binding free energy of OI_13, OI_66, and OI_78 were impressive; therefore, these three molecules could be potential inhibitors. It was unequivocally demonstrated that each chosen hit suitably fitted in the active site cavity. Also, it was noted that the binding posture of each of the chosen (yellow-colored) hits is similar to that of the reference inhibitor acarbose (green color). The active site binding posture of selected hits is comparable to that of the known alpha-glucosidase inhibitor acarbose, revealing that selected hits are not false positives. Most of the hits selected were glycosides in nature, and the *n*-butanol fraction may be the source of these compounds (Nassar et al., 2013, Akowuah
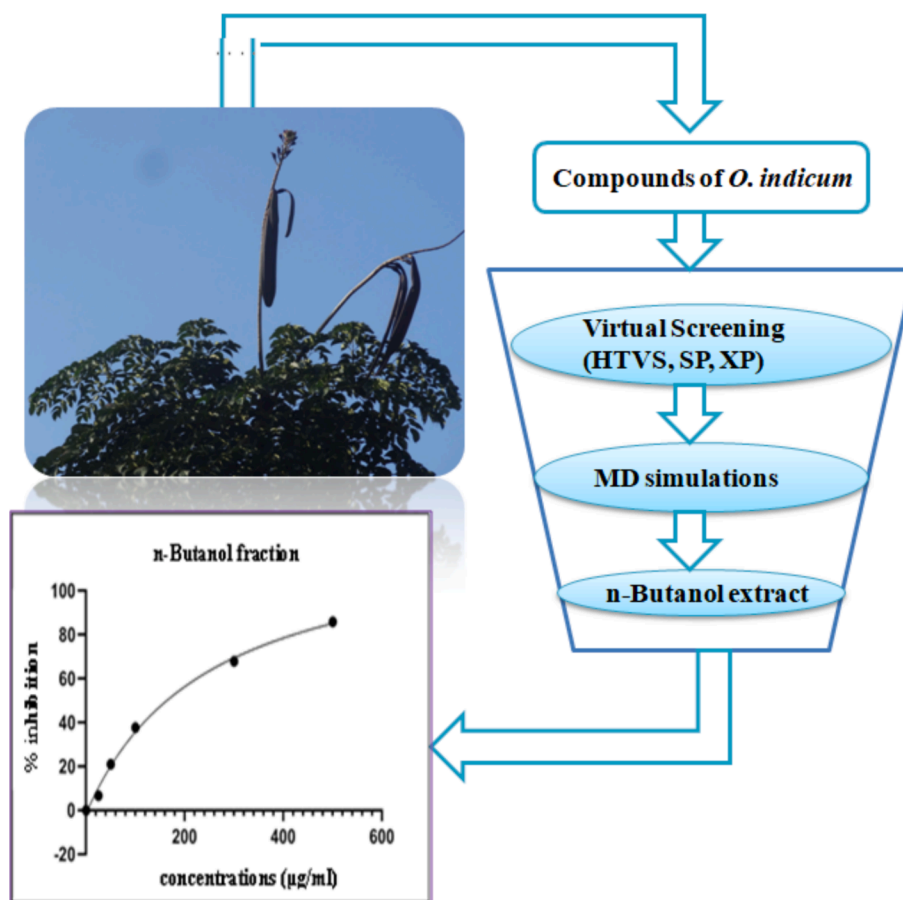
Fig. 10. Diagrammatic representation of the present study.

et al., 2002). Based on the docking score, interacting amino acid residues and MM-GBSA dG bind energy calculated from VS, the OI_13, OI_66, and OI_78 protein–ligand complexes and standard inhibitor acarbose-protein complex were subjected to 100 ns molecular dynamics (MD) simulation. The highest binding affinity of compounds predicted by Swargiary *et al.* against α-glycosidase was − 8.5 kcal/mol, which was not found impressive as the GC–MS result shows only for volatile compounds. The study showed that the leaf extract has the potential for α-glucosidase inhibitory activity (Swargiary & Daimari, 2020). The standard α-glucosidase inhibitors acarbose, maglitol, and voglibose are highly polar in nature. However, GC–MS of previously reported compounds (Swargiary & Daimari, 2020) are comparatively non-polar. On the other hand, the potential compounds reported in the present study were highly polar in nature, and their binding affinities are far better than those reported (−8.5 kcal/mol) earlier.

The average RMSD of OI_13 binding protein calculated from MD trajectories was 1.882 Å less than the average RMSD of 2.414 Å of acarbose binding protein. Similarly, the average RMSD of OI_78 bound protein was 2.633, and the RMSF of OI_78 bound protein residues was 1.896 Å, close to the average RMSF of acarbose binding protein. The orders of the RMSD changes within the range of 1.0–3.0 Å are perfectly acceptable for small, globular proteins (Junejo et al., 2021).

During simulation, the RMSD and RMSF of selected compounds revealed stable protein–ligand interactions. The interacting amino acid residues ASP-199, ASN-258, and ASP-327 were found to be common for both known inhibitors and OI_13. On the occasion of OI_66, the residues common to acarbose were found to be ASP-199, ASN-258, and GLU-283. In the case of OI_78, only one amino residue, ASP-199, was found to be common to known inhibitors interacting with the enzyme. Both the compounds OI_13 and OI_66 showed at least three common interacting

residues similar to standard inhibitor acarbose. The binding free energy of selected hits OI_13 and OI_66 was more significant than the known inhibitor acarbose. Therefore, these two selected hits could serve as potential α-glucosidase inhibitors in the field of pharmaceutical development.

The selected compounds OI_13, OI_16, OI_20, OI_43, and OI_44 were found to be flavone glycosides in nature; in addition, the compounds OI_66 and OI_78 were also found to be glycosides. Literature studies reveal that the *n*-butanol fraction often contains an impressive number of glycosides (Akowuah et al., 2002, Nassar et al., 2002, Cui et al., 2012), and several researchers also studied the α-glucosidase inhibitory activity of *n*-butanol extracts of plant materials (Ajiboye et al., 2019, Kamran et al., 2024). Therefore, the *n*-butanol fraction was selected to evaluate the α-glucosidase inhibitory activity of the plant under study. Moreover, *n*-butanol fraction residue was found to be highly polar in nature due to being readily soluble in aqueous media used for *in vitro* study. The IC$_{50}$ value of standard α-glucosidase inhibitor acarbose was 89.16 μg/ml. On the other hand, the IC$_{50}$ value of the *n*-butanol fraction of methanol extract was 248.1 μg/ml, showing less inhibitory activity as it comprises a mixture of compounds compared to acarbose, a single compound. The use of medicinal plants with anti potential in typeII patients is a common practice worldwide. Plant-based secondary metabolites may act on various carbohydrate metabolism pathways, inducing insulin secretion, inhibiting carbohydrate digestion, reducing the rate of monosaccharide production, or delaying its absorption in the intestine. The α-Glucosidase enzyme is one of the key enzymes in our digestive system that releases monosaccharides from disaccharides and oligosaccharides, hence elevating the postprandial blood glucose level. Therefore, α-Glucosidase inhibition is an effective way to delay absorption and also prevent high postprandial blood glucose levels, which

may suppress diabetes progression. Various drug molecules like acarbose, voglibose, and miglitol, the common α-glucosides inhibitors, are used to manage type II diabetes (Yao et al., 2024, Guo et al., 2022).

Mishra *et. al.* reported the presence of 15 spots through HPTLC profiling of *O. indicum* seed extracts, and the highest area percentage of one component was found to be 71.85 % w/w at R_f 0.88 (Mishra et al., 2018). The seed extract significantly reduced blood glucose levels in rats with chemically induced diabetes (Mishra et al., 2018). The mechanism behind the anti-diabetic activity was not addressed in the above study. Unlike Mishra *et. al.*, in our study, we sought to demonstrate the anti-diabetic property of the *n*-butanol fraction of *O. indicum* bark extract by α-glucosidase inhibition. Most potential inhibitors in this study were found to be glycosides structurally resembling the well-known inhibitor acarbose. Moreover, the residue obtained from the *n*-butanol fraction was found to be soluble in aqueous media, and it could be assumed as another interesting finding of this study. In this context, it is also required to mention the limitations of the present study due to restrictions on the literature-based compounds; thus, future research needs to be focused on the isolation of compounds from *n*-butanol fraction along with preclinical study design to identify and structural elucidation of bioactive molecules of this plant.

Like known inhibitors, the human oral absorption and percentage of human oral absorption for most of the compounds were poor. The α-glucosidase breaks carbohydrates into absorbable monosaccharides located in the small intestine's brush border. The use of these compounds as α-glucosidase inhibitors is encouraged by the decreased absorption of these compounds due to the enzyme functions in the intestines. The poor oral absorption of prospective molecules in humans encourages the implementation of this *n*-butanol fraction as an anti-diabetes medicine, followed by in vivo and toxicity testing.

5. Conclusions

O. indicum was traditionally said to have anti properties, but no scientific validation was carried out in support of this claim. The current investigation aims to predict and identify α-glucosidase inhibitors from the known compounds of *O. indicum* using a rational drug design approach. Molecular docking analysis showed the presence of seven compounds OI_13, OI_66, OI_16, OI_44, OI_43, OI_20, and OI_78, which have an excellent binding affinity towards α-glucosidase and even better than well-known inhibitor acarbose. The 100 ns MD simulation analysis of the top three inhibitors confirmed stable protein–ligand interactions. The MM-GBSA dG binding energy of OI_13, OI_66 and known inhibitor acarbose was found as −69.093, −62.950, and −53.055 kcal/mol, respectively. The MM-GBSA dG binding energy of compounds OI_13 and OI_66 was far better than the MM-GBSA dG binding energy of known inhibitor acarbose. The wet lab experiment also validated the molecular docking and dynamic study results. The inhibition of α-glucosidase in the presence of standard pure inhibitor acarbose at 100 μg/ml was found to be 57.78 %, whereas the inhibition for *n*-butanol fraction of *O. indicum* at 100 μg/ml was 37.7 %, though it contains a mixture of phytoconstituents. All potential phytoconstituents of the *n*-butanol fraction are assumed to be highly polar in nature, and simultaneously, like the known inhibitor acarbose, the percentages of predicted human oral absorption were found to be poor. This finding is identified to be an awe-inspiring part of this study. Thus, the current study supports that the aqueous edible plant extract may be utlized for managing diabetes in humans after further thorough preclinical and toxicity studies. More studies are needed to purify and identify the bioactive molecules and perform preclinical trials in order to create innovative anti- pharmaceutical compositions.

Funding

CRediT authorship contribution statement

Samhita Bhaumik: Formal analysis, Project administration. **Alekhya Sarkar:** Investigation, Methodology. **Sudhan Debnath:** Conceptualization, Writing – review & editing. **Bimal Debnath:** Supervision, Writing – review & editing. **Rajat Ghosh:** Software, Supervision. **Magdi E.A. Zaki:** Data curation, Funding acquisition. **Sami A. Al-Hussain:** Funding acquisition, Validation.

Declaration of competing interest

The authors declare that they have no known competing financial interests or personal relationships that could have appeared to influence the work reported in this paper.

Acknowledgments

Appendix A. Supplementary material

Supplementary data to this article can be found online at https://doi.org/10.1016/j.jsps.2024.102095.

References

Ajiboye, B.O., Ojo, O.A., Fatoba, B., Afolabi, O.B., Olayide, I., Okesola, M.A., Oyinloye, B. E., 2019. In vitro antioxidant and enzyme inhibitory properties of the n-butanol fraction of Senna podocarpa (Guill. and Perr.) leaf. J. Basic Clin. Physiol. Pharmacol. 31 (1), 25. https://doi.org/10.1515/jbcpp-2019-0123.

Akowuah, G.A., Sadikun, A., Mariam, A., 2002. Flavonoid Identification and Hypoglycaemic Studies of the Butanol Fraction from *Gynura procumbens*. Pharm. Biol. 40 (6), 405–410. https://doi.org/10.1076/phbi.40.6.405.8440.

Alam, A., Ali, M., Latif, A., Rehman, N.U., Saher, S., Zainab, F., Khan, A., Ullah, S., Ullah, O., Halim, S.A., Sani, F., Al-Harrasi, A., Ahmad, M., 2022. Novel Bis-Schiff's base derivatives of 4-nitroacetophenone as potent α-glucosidase agents: Design, synthesis and in silico approach. Bioorg. Chem. 128, 106058 https://doi.org/10.1016/j.bioorg.2022.106058.

Auiewiriyanukul, W., Saburi, W., Kato, K., Yao, M., Mori, H., 2018. Function and structure of GH13_31 alpha-glucosidase with high alpha-(1→4)-glucosidic linkage specificity and transglucosylation activity. FEBS Lett. 592, 2268–2281. https://doi.org/10.1002/1873-3468.13126.

Bhatia, A., Singh, B., Arora, R., Arora, S., 2019. In vitro evaluation of the α-glucosidase inhibitory potential of methanolic extracts of traditionally used antidiabetic plants. BMC Complementary Altern. Med. 19, 1–9. https://doi.org/10.1186/s12906-019-2482-z.

Chen, J., Li, X., Liu, H., Zhong, D., Yin, K., Li, Y., Zhu, L., Xu, C., Li, M., Wang, C., 2023a. Bone marrow stromal cell-derived exosomal circular RNA improves diabetic foot ulcer wound healing by activating the nuclear factor erythroid 2-related factor 2 pathway and inhibiting ferroptosis. Diabetic Medicine: J. Br. Diabet. Assoc. 40 (7), e15031.

Chen, R., Xu, S., Ding, Y., Li, L., Huang, C., Bao, M., Li, S., 2023b. Wang Q. Dissecting causal associations of type 2 diabetes with 111 types of ocular conditions: a Mendelian randomization study. Front. Endocrinol. (lausanne) 22, 14, 1307468. https://doi.org/10.3389/fendo.2023.1307468.

Chhetri, D.R., Parajuli, P., Subba, G.C., 2005. Antidiabetic plants used by Sikkim and Darjeeling Himalayan tribes India. J. Ethnopharmacol. 99 (2), 199–202. https://doi.org/10.1016/j.jep.2005.01.058.

Cui, E.J., Song, N.Y., Shrestha, S., et al., 2012. Flavonoid glycosides from cowpea seeds (Vigna sinensis K.) inhibit LDL oxidation. Food Sci. Biotechnol. 21, 619–624. https://doi.org/10.1007/s10068-012-0080-7.

Deka, D.C., Vimal, K., Chandan, P., Kamal, K., Gogoi, B.J., Singh, L., Srivastava, R.B., 2013. *Oroxylum indicum*–a medicinal plant of North East India: An overview of its nutritional, remedial, and prophylactic properties. J. Appl. Pharma. Sci. 3 (Suppl 1), S104–S112. https://doi.org/10.7324/JAPS.2013.34.S19.

Desmond Molecular Dynamics System, Shaw, D. E., Research, 2021. Maestro-Desmond Interoperability Tools, Schrödinger, New York.

Dinda, B., SilSarma, I., Dinda, M., Rudrapaul, P., 2015. Oroxylum indicum (L.) Kurz, an important Asian traditional medicine: from traditional uses to scientific data for its commercial exploitation. J. Ethnopharmacol. 23 (161), 255–278. https://doi.org/10.1016/j.jep.2014.12.027.

Dirir, A.M., Daou, M., Yousef, A.F., Yousef, L.F., 2022. A review of alpha-glucosidase inhibitors from plants as potential candidates for the treatment of type-2 diabetes. Phytochem. Rev. 21 (4), 1049–1079. https://doi.org/10.1007/s11101-021-09773-1.

Feingold, K. R., 2000. Oral and Injectable (Non-Insulin) Pharmacological Agents for the Treatment of Type 2 Diabetes (2022). In: Feingold, K. R., Anawalt, B., Blackman, M. R., Boyce, A., Chrousos, G., Corpas, E., de Herder, W. W., Dhatariya, K., Dungan, K., Hofland, J., Kalra, S., Kaltsas, G., Kapoor, N., Koch, C., Kopp, P., Korbonits, M., Kovacs, C. S., Kuohung, W., Laferrère, B., Levy, M., McGee, E. A., McLachlan, R., New, M., Purnell, J., Sahay, R., Singer, F., Sperling, M. A., Stratakis, C. A., Trence, D. L., Wilson, D. P. editors. 2000. Endotext [Internet]. South Dartmouth (MA): MDText. com, Inc. PMID: 25905364.

Friesner, R.A., Banks, J.L., Murphy, R.B., Halgren, T.A., Klicic, J.J., Mainz, D.T., Repasky, M.P., Knoll, E.H., Shaw, D.E., Shelley, M., Perry, J.K., Francis, P., Shenkin, P.S., 2004. Glide: a new approach for rapid, accurate docking and scoring. 1. Method and assessment of docking accuracy. J. Med. Chem. 47, 1739–1749.

Friesner, R.A., Murphy, R.B., Repasky, M.P., Frye, L.L., Greenwood, J.R., Halgren, T.A., Sanschagrin, P.C., Mainz, D.T., 2006. Extra precision glide: docking and scoring incorporating a model of hydrophobic enclosure for protein-ligand complexes. J. Med. Chem. 49, 6177–6196.

Gul, S., Jan, F., Alam, A., Shakoor, A., Khan, A., AlAsmari, A. F., Alasmari, F., Khan, M., Bo L. 2024. Synthesis, molecular docking and DFT analysis of novel bis-Schiff base derivatives with thiobarbituric acid for α-glucosidase inhibition assessment. *Sci Rep*. 10, 14(1):3419. 10.1038/s41598-024-54021-z.

Guo, W., Zhang, Z., Li, L., Liang, X., Wu, Y., Wang, X., Ma, H., Cheng, J., Zhang, A., Tang, P., Wang, C.Z., Wan, J.Y., Yao, H., Yuan, C.S., 2022. Gut microbiota induces DNA methylation via SCFAs predisposing obesity-prone individuals to diabetes. Pharmacol. Res. 182, 106355 https://doi.org/10.1016/j.phrs.2022.106355.

Halgren, T.A., Murphy, R.B., Friesner, R.A., Beard, H.S., Frye, L.L., Pollard, W.T., Banks, J.L., 2004. Glide: a new approach for rapid, accurate docking and scoring. 2. Enrichment factors in database screening. J. Med. Chem. 47, 1750–1759.

Hevener, K.E., Zhao, W., Ball, D.M., Babaoglu, K.Q.J., White, S.W., Lee, R.E., 2009. Validation of molecular docking programs for virtual screening against dihydropteroate synthase. J. Chem. Inf. Model. 49 (2), 444–460. https://doi.org/10.1021/ci800293n.

Jorgensen, W.L., Maxwell, D.S., Tirado-Rives, J., 1996. Development and testing of the OPLS all atom force field on conformational energetics and properties of organic liquids. J. Am. Chem. Soc. 118 (45), 11225–11236. https://doi.org/10.1021/ja9621760.

Junejo, J.A., Zaman, K., Rudrapal, M., Celik, I., Attah, E.I., 2021. Antidiabetic bioactive compounds from Tetrastigma angustifolia (Roxb.) Deb and Oxalis, debilis, Kunth validation of ethnomedicinal claim by in vitro and in silico studies. South African J Bot. 143, 164–175.

Junge, B., Matzke, M., Stoltefuss, J., 1996. Chemistry and structure-activity relationships of glucosidase inhibitors, In Kuhlman Journal Puls W (eds): Oral Antidiabetics, Berlin, Springer-Verlag. 411.

Kalibaeva, G., Ferrario, M., Ciccotti, G., 2003. Constant pressure-constant temperature molecular dynamics: A correct constrained NPT ensemble using the molecular virial. *Molecular Physics*. 101(6), 765–778. 10.1080/ 0026897 0210000 44025.

Kamran, S. H., Ahmad, M., Ishtiaq, S., Ajaib, M., Razashah, S. H., Shahwar, D. E., 2024. Metabolite profiling and biochemical investigation of the antidiabetic potential of Loranthus pulverulentus Wall n-butanol fraction in diabetic animal models. *J. Ethnopharmacol.* 10 318(Pt A), 116963. 10.1016/j.jep.2023.116963.

Kato, K., Saburi, W., Yao, M., 2018. Crystal structure of Alpha-glucosidase in complex with maltose. PDB. https://doi.org/10.2210/pdb5ZCC/pdb.

Kevin, J., Bowers, E. C., Huafeng, X., Ron O. D., Michael, P., Eastwood, B. A., Gregersen, J. L., Klepeis, I. K., Mark, A. M., Federico, D. S., John, K., Salmon, Y. S., David, E. S., 2006. Scalable Algorithms for Molecular Dynamics Simulations on Commodity Clusters, Proceedings of the ACM/IEEE Conference on Supercomputing (SC06), Tampa, Florida, 11-17.

Khan, M., Ahad, G., Alam, A., Ullah, S., Khan, A., Kanwal, Salar, U., Wadood, A., Ajmal, A., Khan, KM., Perveen, S., Uddin, J., Al-Harrasi, A., 2023. Synthesis of new bis (dimethylamino)benzophenone hydrazone for diabetic management: In-vitro and in-silico approach. *Heliyon*. 4;10(1):e23323. 10.1016/j.heliyon.2023.e23323.

Li, J., Abel, R., Zhu, K., Cao, Y., Zhao, S., Friesner, R.A., 2011. The VSGB 2.0 model: a next generation energy model for high resolution protein structure modelling. Proteins 79, 2794–2812.

Li, J.M., Li, X., Chan, L.W.C., Hu, R., Zheng, T., Li, H., Yang, S., 2023. Lipotoxicity-polarised macrophage-derived exosomes regulate mitochondrial fitness through Miro1-mediated mitophagy inhibition and contribute to type 2 diabetes development in mice. Diabetologia 66 (12), 2368–2386. https://doi.org/10.1007/s00125-023-05992-7.

Liang, D., Cai, X., Guan, Q., Ou, Y., Zheng, X., Lin, X., 2023a. Burden of type 1 and type 2 diabetes and high fasting plasma glucose in Europe, 1990–2019: a comprehensive analysis from the global burden of disease study 2019. Front Endocrinol (lausanne). 13 (14), 1307432. https://doi.org/10.3389/fendo.2023.1307432.

Liang, X., Zhang, J., Wang, Y., Wu, Y., Liu, H., Feng, W., Si, Z., Sun, R., Hao, Z., Guo, H., Li, X., Xu, T., Wang, M., Nan, Z., Lv, Y., Shang, X., 2023b. Comparative study of microvascular structural changes in the gestational diabetic placenta. Diab. Vasc. Dis. Res. 20 (3) https://doi.org/10.1177/14791641231173627.

Libman, A., Bouamanivong, S., Southavong, B., Sydara, K., Soejarto, D.D., 2006. Medicinal plants: an important asset to health care in a region of Central Laos. J. Ethnopharmacol. 106 (3), 303–311. https://doi.org/10.1016/j.jep.2005.11.034.

Lilkova, E. *et al.*, 2015. The PyMOL Molecular Graphics System, Version 2.0 Schrodinger, LLC.

Mark, P., Nilsson, L., 2001. Structure and dynamics of the TIP3P, SPC, and SPC/E water models at 298 K. Chem. A Eur. J. 105 (43), 9954–9960. https://doi.org/10.1021/jp003020w.

Martyna, G.J., 1994. Remarks on Constant-temperature molecular dynamics with momentum conservation. Phys. Rev. E Stat. Phys. Plasmas Fluids Relat Interdiscip. Topics 50 (4), 3234–3236. https://doi.org/10.1103/physreve.50.3234.

Mishra, S. B., Simon, M., Mukerjee, A., Rani, S., Parashar, T., 2018. Phytochemical Investigation and Antidiabetic Activity of *Oroxylum Indicum Vent*. Seed, International Conference on New Horizons in Green Chemistry & Technology (ICGCT). SSRN: https://ssrn.com/abstract=3298676 or 10.2139/ssrn.3298676.

Nassar, M. I., Aboutabl, el-S. A., Eskander, D. M., Grace, M. H., El-Khrisy, E. D., Sleem, A. A., 2002. Flavonoid glycosides and pharmacological activity of *Amphilophium paniculatum*. Pharmacognosy Res. 5(1), 17-21. 10.4103/0974-8490.

Nassar, M. I., Aboutabl, el-SA., Eskander, D. M., Grace, M. H., El-Khrisy, E. D., Sleem, A. A., 2013. Flavonoid glycosides and pharmacological activity of *Amphilophium paniculatum*. Pharmacognosy Res. 5(1), 17-21. 10.4103/0974-8490.105643.

Ong, K.L., 2023. GBD 2021 Diabetes Collaborators, Global, regional, and national burden of diabetes from 1990 to 2021, with projections of prevalence to 2050: a systematic analysis for the Global Burden of Disease Study 2021. Lancet 402, 203–234. https://doi.org/10.1016/S0140-6736(23)01301-6.

Pistia-Brueggeman, G., Hollingsworth, R.I., 2001. A preparation and screening strategy for glycosidase inhibitors. Tetrahedron 57, 8773–8778.

Rydén, L., Grant, P.J., Anker, S.D., Berne, C., Cosentino, F., et al., 2013. ESC Guidelines on diabetes, pre-diabetes, and cardiovascular diseases developed in collaboration with the EASD: the Task Force on diabetes, pre-diabetes, and cardiovascular diseases of the European Society of Cardiology (ESC) and developed in collaboration with the European Association for the Study of Diabetes (EASD). Eur. Heart Journal. 34 (39), 3035–3087. https://doi.org/10.1093/eurheartj/eht108.

Saeedi, P., Petersohn, I., Salpea, P., Malanda, B., Karuranga, S., Unwin, N., Colagiuri, S., Guariguata, L., Motala, A. A., Ogurtsova, K., Shaw, J. E., Bright, D., Williams, R., 2019. IDF Diabetes Atlas Committee. Global and regional diabetes prevalence estimates for 2019 and projections for 2030 and 2045: Results from the International Diabetes Federation Diabetes Atlas, 9th edition, Diabetes. Res. Clin. Pract. 157,107843. 10.1016/j.diabres.2019.107843.

Schrödinger, 2021, LigPrep, LLC, New York.

Schrödinger, 2021, Maestro LLC, New York.

Schrödinger, QikProp, 2021, LLC, New York.

Shen, X., Gai, Z., Kato, K., Yao, M., 2015a. Crystal structure of alpha-glucosidase. PDB. https://doi.org/10.2210/pdb3WY1/pdb.

Shen, X., Gai, Z., Kato, K., Yao, M., 2015b. Crystal structure of alpha-glucosidase in complex with glucose. PDB. https://doi.org/10.2210/pdb3WY2/pdb.

Shen, X., Saburi, W., Gai, Z., Kato, K., Ojima-Kato, T., Yu, J., Komoda, K., Kido, Y., Matsui, H., Mori, H., Yao, M., 2015c. Structural analysis of the alpha-glucosidase HaG provides new insights into substrate specificity and catalytic mechanism. Acta Crystallogr. D Biol. Crystallogr. 71, 1382–1391. https://doi.org/10.1107/S139900471500721X.

Su, M., Hu, R., Tang, T., Tang, W., Huang, C., 2023. Review of the correlation between Chinese medicine and intestinal microbiota on the efficacy of diabetes mellitus. Front. Endocrinol. 13 https://doi.org/10.3389/fendo.2022.1085092.

Swargiary, A., Daimari, M., 2020. Identification of bioactive compounds by GC-MS and α-amylase and α-glucosidase inhibitory activity of Rauvolfia tetraphylla L. and Oroxylum indicum (L.) Kurz: an in vitro and in silico approach. Clin. Phytosci. 6, 75.

Toukmaji, A.Y., Board, J.J., Ewald, A., 1996. Summation techniques in perspective: a survey. Computational Phys. Commun. 95, 73–92. https://doi.org/10.1016/0010-4655(96)00016-1.

Wang, C., Wang, S., Wang, Z., Han, J., Jiang, N., Qu, L., Xu, K., 2024. Andrographolide regulates H3 histone lactylation by interfering with p300 to alleviate aortic valve calcification. Br. J. Pharmacol. 20 https://doi.org/10.1111/bph.16332.

Xiao, D., Guo, Y., Li, X., Yin, J.Y., Zheng, W., Qiu, X.W., Xiao, L., Liu, R.R., Wang, S.Y., Gong, W.J., Zhou, H.H., Liu, Z.Q., 2016. The Impacts of SLC22A1 rs594709 and SLC47A1 rs2289669 Polymorphisms on Metformin Therapeutic Efficacy in Chinese Type 2 Diabetes Patients. Int. J. Endocrinol. https://doi.org/10.1155/2016/4350712.

Yang, Y.Y., Chen, Z., Yang, X.D., Deng, R.R., Shi, L.X., Yao, L.Y., Xiang, D.X., 2021. Piperazine ferulate prevents high-glucose-induced filtration barrier injury of glomerular endothelial cells. Exp. Ther. Med. 22 (4), 1175. https://doi.org/10.3892/etm.2021.10607.

Yao, H., Zhang, A., Li, D., Wu, Y., Wang, C.Z., Wan, J.Y., Yuan, C.S., 2024. Comparative effectiveness of GLP-1 receptor agonists on glycaemic control, body weight, and lipid profile for type 2 diabetes: systematic review and network meta-analysis. BMJ (clinical Research Ed.) 384, e076410.

Zhou, Y., Chai, X., Yang, G., Sun, X., Xing, Z., 2023. Changes in body mass index and waist circumference and heart failure in type 2 diabetes mellitus. Front Endocrinol (lausanne). 21 (14) https://doi.org/10.3389/fendo.2023.1305839.

Zhou, L., Liu, Y., Sun, H., Li, H., Zhang, Z., Hao, P., 2022. Usefulness of enzyme-free and enzyme-resistant detection of complement component 5 to evaluate acute myocardial infarction. Sens. Actuators B 369, 132315. https://doi.org/10.1016/j.snb.2022.132315.